Biochemical and Biophysical Characterization of Inhibitor Binding to Caspase-3 Reveals Induced Asymmetry

Ann Aulabaugh,*,‡ Bhupesh Kapoor,‡ Xinyi Huang,‡ Paul Dollings,‡ Wah-Tung Hum,‡ Annette Banker,‡ Andrew Wood,§ and George Ellestad‡

Department of Chemical and Screening Sciences, and Department of Neuroscience, 401 N. Middletown Road, Wyeth Research, Pearl River, New York 10965

Received January 11, 2007; Revised Manuscript Received May 31, 2007

ABSTRACT: Activation of the caspase family of cysteine proteases results in the deregulation of cellular homeostasis and apoptosis. This deregulation is a key factor in the development of Alzheimer's disease, Parkinson's disease, and cancer. Thus, the caspases are important drug targets for the therapeutic intervention of a number of pathological states involving inflammation and apoptosis. In this article, we report the results of inhibition kinetics and binding studies utilizing fluorescence spectroscopy and isothermal titration calorimetry to characterize the mechanism of interaction of caspase-3 with three different classes of inhibitors: peptidomimetics, isatins, and pyrimidoindolones. The peptidomimetics and pyrimidoindolones bind to both active sites of the caspase-3 homodimer with equal affinity and favorable enthalpic and entropic binding contributions. Enzyme activity is abolished when both active sites are occupied with the above inhibitors. In contrast, the isatins bind to caspase-3 with significant heat release (−12 kcal/mol) and negative entropy. In addition, enzyme activity is abolished upon isatin binding to one active site of the homodimer resulting in half-site reactivity. Our studies provide important mechanistic insight into inhibitor interactions with caspase-3 and a way to characterize inhibitor interactions that may not be readily apparent from the crystal structure.

Initiation and execution of apoptosis and inflammatory responses are dependent upon the precise coordination and regulation of the caspase family of cysteine proteases (*1*−*4*). Fourteen caspases have been identified that can be divided into three functional groups associated with inflammation or apoptosis. One group associated with inflammation contains caspases-1, -4, and -5. The other two groups associated with apoptosis include the initiator caspases (-8, -9, and -10) and the effector caspases (-3, -6, and -7). The initiator caspases are activated by extrinsic or intrinsic apoptotic stimuli and then proceed to activate the effector caspases. All effector caspases are expressed as cytosolic zymogens that are subsequently cleaved at specific intrachain sites. Intrachain cleavage is essential for the activation of the dimeric effector caspases; however, a proximity-induced dimerization model has been proposed for initiator caspase activation (*5*−*7*). Activated caspases contain a catalytic dyad comprised of a nucleophilic cysteine and a histidine, and have a strict specificity for cleavage after aspartyl residues. Substrate specificity is regulated by the sequence of four amino acids amino-terminal to the cleavage site as effector caspases cleave after DEVD sequences while activator caspases cleave after (V/I/L)EXD sequences. The effector caspases carry out the specific cleavage of protein targets within the cell that are associated with cellular homeostasis. The central role of caspases in apoptosis has made these proteases an important target for therapeutic intervention in stroke, ischemia, neurodegenerative disorders such as Alzheimer's disease, cancer, and inflammatory diseases (*3*, *4*). Most of the inhibitors to date are peptide-based and have been used to validate the role of caspases in many diseases, while much effort has been devoted to developing nonpeptide reversible inhibitors that bind at the active site (*8*−*10*).

Three-dimensional structures of active caspase-1 (*11*), caspase-3 (*12*), and caspase-7 (*13*) in the absence of bound inhibitor as well as caspase−inhibitor complexes (*11*, *12*, *13*, and reviewed in *14*) have been determined to provide information about inhibitor-induced conformational changes and molecular interactions important for inhibitor potency and specificity. Caspase-3 consists of a homodimer of heterodimers, with each heterodimer containing a small subunit of approximately 10 kDa and a large subunit of approximately 20 kDa (Figure 1). The majority of published caspase−inhibitor structures contain a peptide or protein inhibitor or a small molecule inhibitor bound at the active site. The exception is a class of small molecule inhibitors bound at an allosteric site between the homodimer interface on caspase-7 or caspase-1 that traps the enzyme in a zymogen-like conformation (*15*, *16*). Though detailed structural and kinetic information on the mechanism of inhibitor interactions with caspases have been obtained, little is known about the stoichiometry of caspase inhibition or the thermodynamics of inhibitor binding to caspase that would aid rational drug design.

* Phone: (845)-602-3058. Fax: (845)-602-5687. E-mail: aulabaa@wyeth.com.

‡ Department of Chemical and Screening Sciences.

§ Department of Neurosciences, Princeton, NJ.

10.1021/bi7000505 CCC: $37.00
Published on Web 07/25/2007

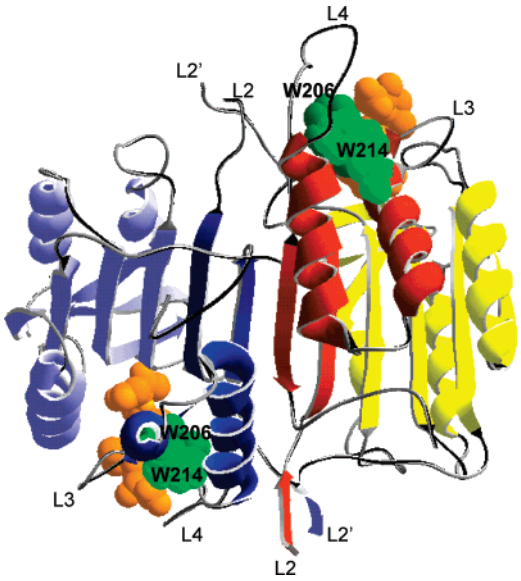

FIGURE 1: Structure of the caspase-3 homodimer bound to Ac-DVAD-FMK (pdb entry 1CP3). The small subunits are colored blue and brown, and the two corresponding large subunits are colored light blue and yellow, respectively. The loops comprising the substrate-binding region on the large subunit (L2, L3, and L4) and the small subunit (L2′) are labeled. The inhibitor (orange) and residues W206 and W214 (green) are shown.

In this study, we have employed inhibition kinetics, isothermal titration calorimetry (ITC[1]) and fluorescence spectroscopy to characterize the thermodynamics and mechanism of caspase-3 interactions with the following three classes of inhibitors: (1) peptidomimetic (Figure 2A and B); (2) isatin (Figure 2C); and (3) pyrmidoindolone (Figure 2D). The results from these studies demonstrate that (1) the peptidomimetics and pyrimidoindolones bind to both active sites of the caspase-3 homodimer with equal affinity; (2) the binding of the peptidomimetics and pyrimidoinolones is enthalpically driven with favorable entropy; (3) isatin binding to caspase-3 is enthalpically driven with unfavorable entropy; and (4) isatin binds to caspase-3 with negative cooperativity and abolishes enzyme activity upon binding to one active site of the homodimer (half-site reactivity).

MATERIALS AND METHODS

Reagents. Caspase substrates (Ac-DEVD-AFC and Ac-YVAD-AFC) were purchased from BIOMOL Research Laboratories (Plymouth Meeting, PA). Standard laboratory reagents were purchased from Sigma, Aldrich, Fluka, and Research Organics.

Protein Expression and Purification. The DNA sequence encoding the caspase-3 catalytic domain (no prodomain) with a C-terminal hexa-His tag was inserted into Vector pET-16b and expressed in *Escherichia coli* BL21 (DE3) cells. Cell pellets were resuspended in 20 mM Tris (pH 8.0), 500 mM NaCl, and 5 mM imidazole. The cell suspension was disrupted by passing the suspension 5 times through a microfluidizer Model 110Y (Microfluidics Corp, Newton, MA). After centrifugation (Sorvall rotor GSA, 13,000 rpm, 30 min at 4 °C), the supernatant was applied to a column of Ni-NTA agarose. Caspase-3 was eluted with a gradient of 5 mM to 150 mM imidazole in the above buffer (20 mM Tris (pH 8.0), 500 mM NaCl, and 5 mM cysteine at pH 8.0). Fractions containing caspase-3 were pooled and concentrated with a Millipore Ultrafree filtration device. The concentrated caspase-3 solution was loaded on a TSK gel G3000sw column (Tosoh Bioscience LLC) and eluted with a buffer of 20 mM PIPES (pH 7.2), 100 mM NaCl, 1 mM EDTA, and 5 mM cysteine. Fractions containing caspase-3 were pooled and concentrated. CHAPS and sucrose were added to a final concentration of 0.1% and 10%, respectively. The purified caspase-3 was greater than 95% pure and showed two subunits of 20 and 10 kDa on reduced SDS−PAGE. The concentration of the purified protein was determined from the absorbance at 280 nm with the extinction coefficient obtained from Sednterp (ϵ_{280} = 24,180 M^{-1} cm^{-1}) (*17*).

Enzyme Assays. Enzyme activity was measured using a fluorescence assay as described previously (*18*). Briefly, caspase-3 was added last to the assay buffer (20 mM Pipes (pH 7.5), 100 mM NaCl, 0.1% CHAPS, 10% sucrose, and 5 mM cysteine) containing 25 μM Ac-DEVD-AFC substrate at room temperature (22 °C) to afford a final enzyme concentration of 0.25 nM. The enzyme concentration is reported as the concentration of heterodimer. The formation of AFC was monitored for 90 min using an excitation wavelength of 400 nm and an emission wavelength of 505 nm on a Molecular Devices GeminiII plate reader.

Inhibition Assays and Active-Site Titrations. The inhibition profile of an inhibitor was determined in the enzyme assays described above. The concentration of Ac-DEVD-AFC was varied from 5 to 75 μM, and the concentration of inhibitor was varied from 0.2 nM to 20 μM. Caspase-3 was added last to initiate the enzyme reaction, which was monitored for at least 1.5 h. Initial rates for the rapidly reversible, competitive isatin inhibitor IST-1 (*19*) were analyzed using eq 1:

$$v_0 = \frac{V_{max}[S]}{[S] + K_M\left(1 + \frac{[I]}{K_i}\right)} \quad (1)$$

where K_M is the Michaelis constant, and V_{max} is the catalytic rate at saturating substrate concentration. The K_i values for the rapidly reversible IST-2 and IST-3 inhibitors were calculated from the IC_{50} values obtained from a dose−response curve at one substrate concentration using eq 2 for competitive inhibition.

$$K_i = \frac{IC_{50}}{\left(1 + \frac{S}{K_M}\right)} \quad (2)$$

Progress curves for time-dependent inhibitors were analyzed using eq 3 (*20*):

$$[P] = v_s t + \frac{v_0 - v_s}{k_{obs}}(1 - e^{-k_{obs}t}) \quad (3)$$

where [*P*] is the product concentration at any time *t*, v_0 and v_s are the initial and final steady-state rates, and k_{obs} is the

[1] Abbreviations: AFC, 7-amino-4-trifluoromethylcoumarin; DMSO, dimethylsulfoxide; FMK, fluoromethylketone; ITC, isothermal titration calorimetry; Pipes, 1,4-piperazinediethanesulfonic acid; CHAPS, 3-[(3-cholamido-propyl)dimethylammonio]-1-propanesulfonic acid; RFU, relative fluorescence unit; UV, ultraviolet.

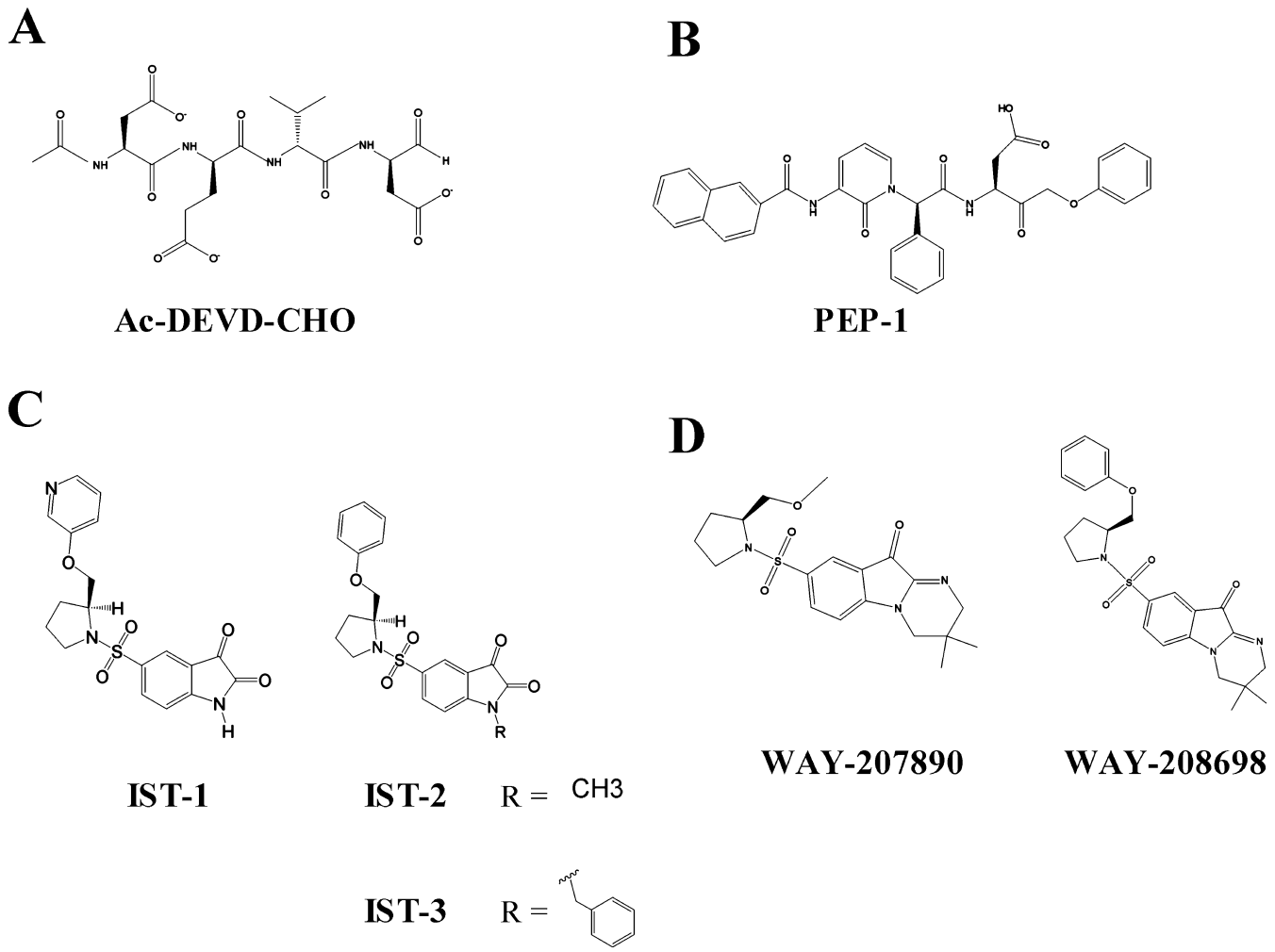

FIGURE 2: Structures of the caspase-3 inhibitors investigated.

apparent first-order rate constant for establishment of the final steady-state equilibrium. The initial and final steady-state rate data were fit using eq 1 to obtain K_i and K_i*, respectively, where K_i represents the inhibition constant of the initial complex, and K_i* is the overall inhibition constant including initial binding and the slow conversion to the tight-binding complex. The data were analyzed using Sigma Plot 2000 Enzyme Kinetics Module from SPSS Science (Richmond, CA).

The stoichiometry of inhibitor inactivation of caspase-3 was determined by active-site titration using the alternative substrate Ac-YVAD-AFC. A fixed concentration of inhibitor (typically 300 to 400 nM) was typically preincubated for 30 min with increasing concentrations of caspase-3 (25 nM to 1.4 μM) in a 96-well microplate. The reactions were initiated with the addition of the substrate Ac-YVAD-AFC (20 μM). Control titrations were performed, where increasing concentrations of caspase-3 were preincubated in buffer.

Fluorescence Titrations. Fluorescence spectroscopy was used to determine the affinity of inhibitor binding to caspase-3. Fluorescence spectra were obtained on a Perkin-Elmer LS50 B instrument. The ligand solution was added stepwise (1 to 2 μL aliquots) to a quartz-cuvette containing 1 mL of 1.5 μM caspase-3 in the assay buffer with 5 mM cysteine. The final concentration of ligand was typically 30 nM to 15 μM for isatins and Ac-DEVD-CHO, 100 nM to 15 μM for pyrmidoindolones, and 400 nM to 15 μM for PEP-1. Ligand control titrations were performed where the ligand solution was added stepwise to buffer alone. Emission spectra (300 to 500 nm) were obtained upon excitation at 295 nm using slit widths of 2 nm after the fluorescence signal had stabilized: typically 10 min. The control titration of inhibitor alone was subtracted from each concentration point, and the ligand-dependent protein fluorescence changes at 350 nm, ΔF, were fitted to the quadratic equation (eq 4) to obtain the apparent dissociation constant (K_d) for the inhibitor−caspase-3 interaction:

$$\Delta F = F_0 - F = \frac{(F_0 - F_{max})([E] + [I] + K_d - \sqrt{([E] + [I] + K_d)^2 - 4[E][I]})}{2[E]} \quad (4)$$

where E is the heterodimer concentration, F_0 is the caspase-3 Trp fluorescence in the absence of compound, F is the observed Trp fluorescence after subtraction of the inhibitor control, and F_{max} is the fluorescence in the presence of saturating concentrations of compound. Control titrations of tryptophanamide with inhibitor were performed to determine whether the compound interfered with tryptophan fluorescence.

Isothermal Titration Calorimetry. Isothermal titration calorimetry experiments were performed using a high-precision VP-ITC titration calorimeter (MicroCal Inc.,

Northhampton, MA). The caspase-3 solution (10 to 15 μM heterodimer) in the calorimetric cell (25 °C) was titrated with the ligand dissolved in the same buffer. Typically, 8 μL aliquots of the ligand were injected 32 times into the caspase-3 solution (20 mM Pipes (pH 7.2), 100 mM NaCl, 1 mM EDTA, 1 mM cysteine, and 0.5% DMSO) or into buffer alone to determine the heat of dilution. The heat released upon ligand binding (ΔH) was determined by integrating the area of each titration peak and subtracting the heat due to dilution and DMSO mismatch prior to data analysis. The presence of a linked protonation−deprotonation reaction upon isatin binding was checked by repeating the titration in PBS, a buffer with an ionization enthalpy (1.2 kcal/mol) lower than Pipes (2.7 kcal/mol) (*21*). Thermodynamic parameters ΔH (enthalpy change), n (stoichiometry), and K_a (association constant) were obtained by nonlinear least-squares fitting of the experimental data using the single set of independent binding sites model of the Origin 5.0 software supplied by MicroCal. The affinity of ligand for caspase-3 is reported as the dissociation constant ($K_d = 1/K_a$). The free energy of binding (ΔG) and entropy (ΔS) were obtained using eqs 5 and 6:

$$\Delta G = - \mathrm{RT} \ln K_a \quad (5)$$

$$\Delta G = \Delta H - T\Delta S \quad (6)$$

where R is the gas constant, and T is the absolute temperature in Kelvin.

UV Spectrophotoscopy of Compound Interaction with Caspase-3. The interaction of isatin IST-1 with caspase-3 was monitored by the decrease in isatin absorbance at 410 nm due to complex formation in an Agilent 8453 UV/vis spectrophotometer. Aliquots of IST-1 inhibitor were added stepwise to caspase-3 (65 μM active heterodimer) and the absorbance at 410 nm recorded after the signal stabilized, typically 5 min. A control titration was performed where compound was added stepwise to buffer alone. The formation of the thiohemiketal complex results in the loss of the 410 nm signal relative to the unreacted control signal, and the amount of isatin that did not react with the active site cysteine (free and noncovalent complex) corresponds to the observed A410 signal. The concentration of the thiohemiketal complex is proportional to the difference between the control A410 and the observed A410 and is calculated using the IST-1 extinction coefficient obtained from the control titration: 501 $M^{-1}cm^{-1}$.

RESULTS

Inhibition and Stoichiometry of Caspase-3 Inactivation. Three classes of known peptide inhibitors were evaluated in the fluorescence enzyme activity assay (Table 1). Results from the initial velocity studies showed that IST-1, PEP-1, WAY-207890, and Ac-DEVD-CHO are competitive inhibitors against the Ac-DEVD-AFC substrate (Supporting Information Figure 1). The steady-state potency and the time-dependent inhibition are in good agreement with previously published results (*18*, *19*, *22*, *23*). The availability of highly purified caspase-3 and the tight-binding properties of the different inhibitors (Table 1) allowed us to determine the stoichiometry of the inhibition of caspase-3 for the different chemical classes by active-site titration. The substrate Ac-YVAD-AFC used in these experiments had a lower k_{cat}/K_M value (~4000-fold lower) than that of Ac-DEVD-AFC that enabled caspase-3 activity measurements up to 1.4 μM heterodimer. The inhibitor was titrated with caspase-3 to reduce any interference that may arise in the fluorescence activity assay if caspase-3 were titrated with the inhibitor. The inhibitor concentration used in the titrations was at least 20 times the steady-state K_i for Ac-DEVD-CHO, isatin, and pyrimidoindolone, and 10 times the K_i for PEP-1 to ensure that tight-binding conditions in the titrations were met. Increasing amounts of caspase-3 were incubated with a fixed concentration of the inhibitor for 30 min prior to the addition of the substrate (Figure 3). In the Ac-DEVD-CHO titration, enzyme activity was completely abolished at caspase-3 heterodimer concentrations lower than inhibitor concentration (Figure 3A). The enzyme activity increased on further addition of caspase-3 and paralleled the increase in the control titration, consistent with the tight-binding behavior of the inhibitor (*24*). The stoichiometry of the interaction was obtained from the intercept of the horizontal axis. As shown in Figure 3A, the intercept for the 400 nM Ac-DEVD-CHO titration was 390 nM caspase-3 heterodimer, corresponding to a 1/1 stoichiometry of inhibitor/active site. Thus, there is stoichiometric binding of Ac-DEVD-CHO, and both active sites on the caspase homodimer need to be occupied by Ac-DEVD-CHO for complete inhibition to occur. The experiments were repeated with peptidomimetic PEP-1, isatin IST-1, and the pyrmidoindolones WAY-207890 and WAY-208698 to determine if similar stoichiometry is observed with these inhibitors. The curvature observed at low enzyme concentration in the titration of IST-1 (Figure 3B) is consistent with the decreased potency of this inhibitor relative to Ac-DEVD-CHO (Table 1). The stoichiometry of the inhibition of PEP-1, WAY-207890, or WAY-208698 with the caspase-3 heterodimer was also 1/1 (Figure 3C and Supporting Information Figure 2). However, different results were obtained for the IST-1 titration. The intercept for the titration of 310 nM IST-1 is approximately 600 nM (Figure 3B), which corresponds to a stoichiometry of inhibitor to caspase-3 heterodimer of 0.5/1. This result with isatin indicates that inhibition can occur with only one active site occupied. To determine if this half-site reactivity was unique to IST-1, two additional isatin analogues, IST-2 and IST-3, were characterized, and both displayed half-site reactivity (Table 1). These experiments were repeated with at least three different batches of purified enzyme and yielded reproducible results.

Table 1: Inhibition Constants and Stoichiometry of Inhibition

compd	K_i[a] (nM)	K_i*[a] (nM)	stoichiometry[c] ([inhibitor]/[active site])
IST-1	16.1 ± 0.98		0.5
IST-2	11 ± 2[b]		0.5
IST-3	2.5 ± 0.5[b]		0.5
PEP-1	165 ± 8		1.0
WAY-207890	265 ± 58	0.61 ± 0.08	1.0
WAY-208698	478 ± 71	0.41 ± 0.11	1.0
Ac-DEVD-CHO	77 ± 43	1.6 ± 0.5	1.0

[a] K_i was calculated from the initial rates, and K_i* was calculated from the steady-state rates for time-dependent inhibitors. [b] K_i was calculated using the following equation for competitive inhibition, $K_i = IC_{50}/(1 + S/K_M)$. [c] Stoichiometry was determined from the intersection of the inhibitor titration curve.

Binding of Caspase-3 and Inhibitors by Fluorescence Spectroscopy. The interaction of inhibitors with caspase-3

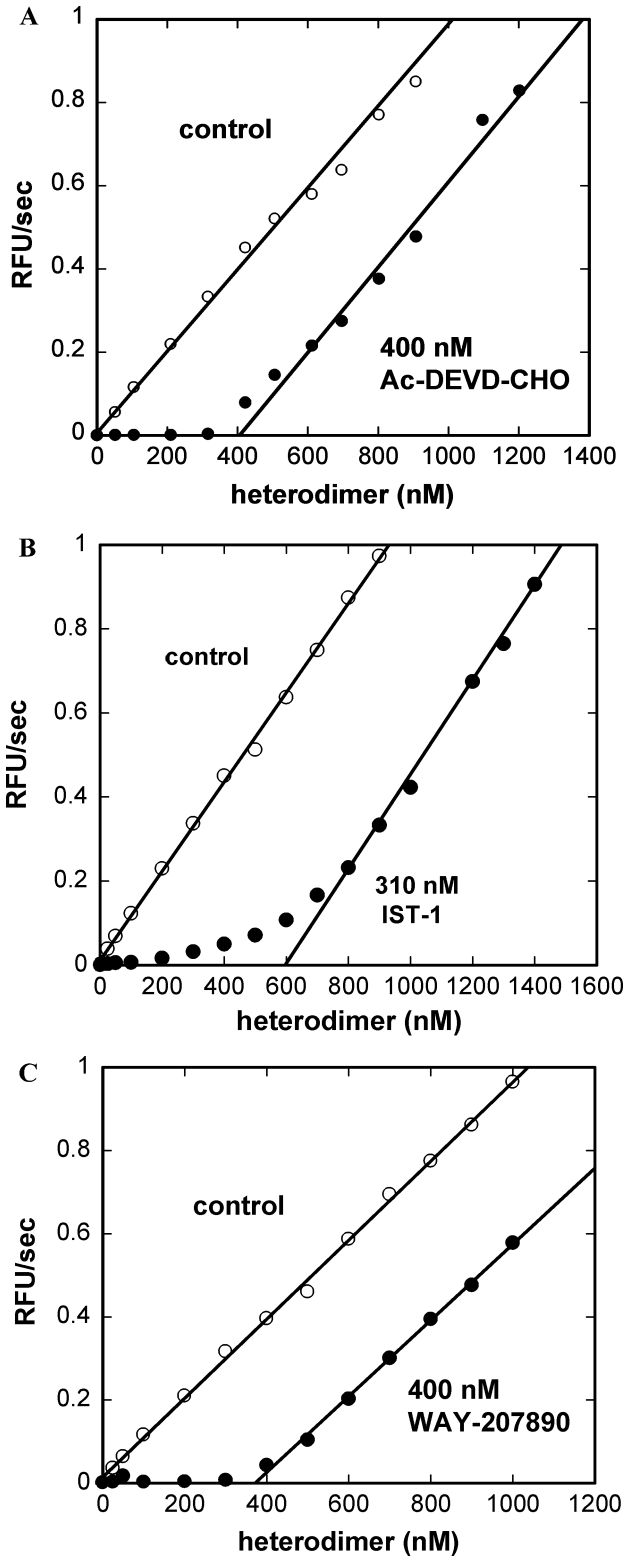

FIGURE 3: Stoichiometry of inhibitor binding to caspase-3 by active-site titration. (A) Peptidomimetic inhibitor Ac-DEVD-CHO (400 nM), (B) IST-1 (310 nM), or (C) WAY-207890 (400 nM) was preincubated for 30 min at room temperature with increasing amounts of caspase-3 (0−1.4 μM heterodimer concentration, ●). Increasing concentrations of caspase-3 were preincubated in buffer for 30 min at room temperature to generate the control curve (○). The enzymatic reaction was initiated by the addition of Ac-YVAD-AFC.

was directly assessed by fluorescence spectroscopy. Caspase-3 contains two tryptophan residues, W206 and W214, located within the active site in the S2 and S4 pockets, respectively (Figure 1). Conformational changes of the two Trp residues are observed in the crystal structures of caspase-3 in the presence of Ac-DEVD-CHO or Ac-DVAD-FMK relative to the crystal structure of unoccupied caspase-3 (*12*). These results imply that intrinsic Trp fluorescence could be a sensitive probe for characterizing inhibitor binding and potency. Sequential addition of aliquots of PEP-1or IST-2 resulted in a decrease of the tryptophan fluorescence quantum yield to greater than 80% (Figure 4). Similar results were obtained with the addition of Ac-DEVD-CHO (Supporting Information Figure 3) or pyrimidoindolone (data not shown). The fluorescence change was proportional to the concentration of the inhibitor−caspase-3 complex, and inhibitor affinity to the protein was obtained from the binding isotherm using eq 4 (Table 2). Control titration of tryptophanamide with ligand indicated that the compounds did not interfere with tryptophan fluorescence at the inhibitor concentrations used in the titrations. Interestingly, a similar extent of tryptophan quenching on the titration of caspase-3 with IST-2 (Figure 4C) was reached at less than 50% of heterodimer concentration. This result implies a conformational change not only at the ligand-occupied active site but also at the unoccupied site.

Thermodynamics of Ligand Binding to Caspase-3 as Measured by ITC. To better understand the thermodynamics of inhibitor binding, isothermal titration calorimetry experiments were performed. The stoichiometry (n), affinity (expressed as the dissociation constant K_d), and the thermodynamic parameters ΔH, ΔG, and ΔS can be obtained from a single experiment to afford a thermodynamic profile for each inhibitor. The stoichiometry data obtained from the ITC experiments (Table 3) are consistent with the steady-state data obtained by the kinetic experiments. However, the K_d obtained by ITC and Trp quenching are intermediate between the initial rate K_i value and the steady-state K_i* value, implying that binding affinity is due to an initial binding step. The shape of the binding isotherms for PEP-1 (Figure 5A), WAY-207890 (Figure 5B), and Ac-DEVD-CHO (data not shown) are consistent with equivalent binding sites on the caspase-3 homodimer, and the data best fit the model for a single class of binding sites. The binding of isatin IST-1 is also consistent with one class of sites, corresponding to half-site reactivity as observed in the active-site titration (Figure 5C). If IST-1 were to bind to the second active site of caspase-3, then K_{d2} would be greater than 15 μM (the protein concentration used in the experiments). The binding of all inhibitors investigated to caspase-3 is enthalpically driven, though significantly greater heat is evolved upon the binding of the isatins (−10 to −12 kcal/mol) compared to PEP-1 or WAY-207890 (−2.46 and −2.75 kcal/mol, respectively; Table 3). Because the ΔG values for pyrimidoindolone and isatin binding to caspase-3 are similar under similar buffer conditions, the large difference in ΔH means WAY-207890 binding is entropically favorable, whereas isatin binding is entropically unfavorable. These results indicate that though the two inhibitors have some structural similarity, the binding stoichiometry and thermodynamics with caspase-3 are different. Omitting sucrose from the binding buffer had no effect on the observed heat of isatin binding. The titration with isatin was repeated using a buffer with a different heat of ionization to determine whether proton transfer during binding may contribute to the observed

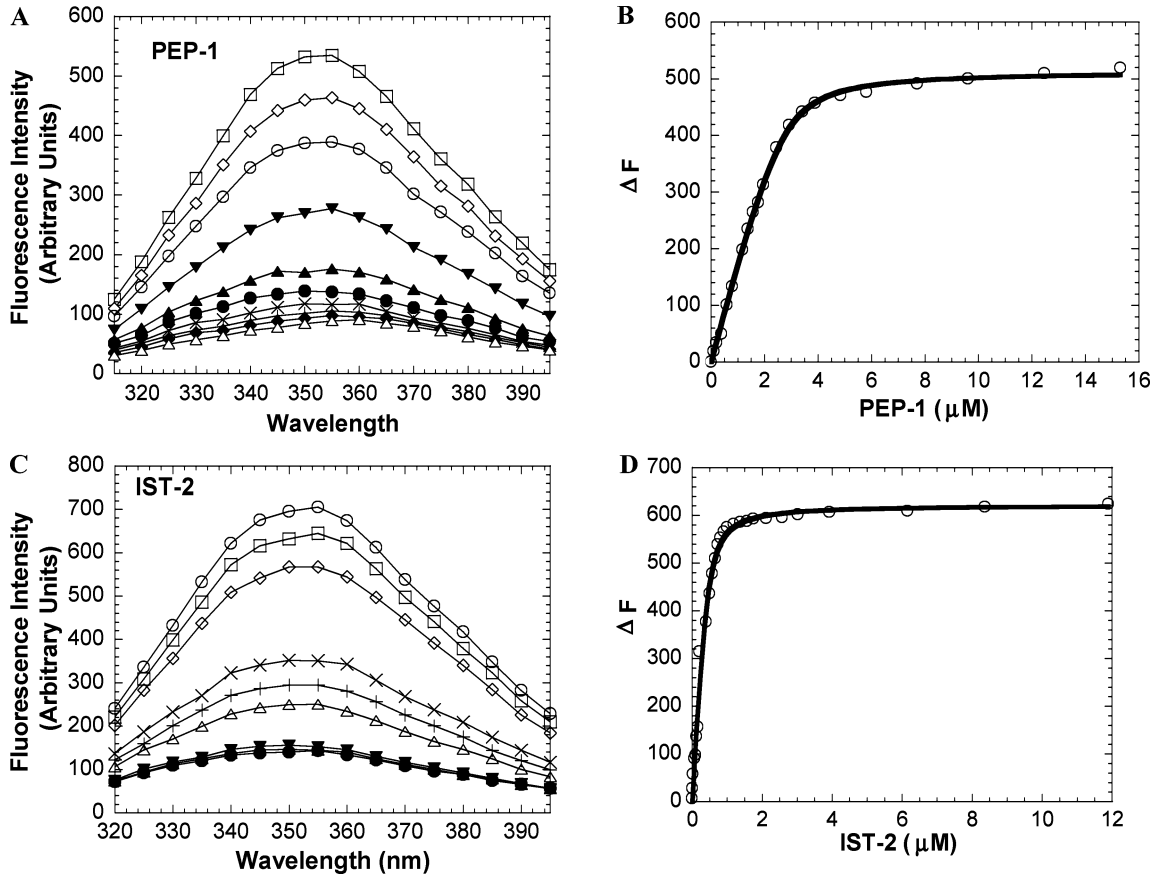

FIGURE 4: Change in intrinsic tryptophan fluorescence of caspase-3 upon the addition of inhibitor. Fluorescence spectra of 1.5 μM caspase-3 in the presence of different concentrations of PEP-1 (A) or IST-2 (C) were obtained upon excitation at 295 nm. (A) The PEP-1 concentrations plotted include 0.4 μM (□), 0.79 μM (◊), 1.38 μM (○), 2.44 μM (▼), 3.41 μM (▲), 4.85 μM (●), 7.72 μM (×), 9.62 μM (+), 12.47 μM (♦), and 15.31 μM (△). (C) The IST-2 concentrations plotted include 0.03 μM (○), 0.10 μM (□), 0.21 μM (◊), 0.50 μM (×), 0.58 μM (+), 0.66 (△), 1.19 μM (▼), 1.57 μM (▲), and 1.75 μM (●). Binding isotherms for PEP-1 (B) or IST-2 (D) were derived from the changes in fluorescence emission, ΔF, with increasing inhibitor concentration. The solid line corresponds to the fit of the data to the quadratic equation.

Table 2: Caspase-3 Inhibitor Potency from Trp Fluorescence Quenching

inhibitor	K_d (nM)
PEP-1	208 ± 21
Ac-DEVD-CHO	51 ± 27
IST-1	87 ± 7
IST-2	58 ± 28
WAY-207890	50 ± 25

enthalpy (Table 3). No change in ΔH was observed upon changing the buffer composition, eliminating proton transfer as a contribution to the binding enthalpy.

We performed a titration experiment of the 1-to-2 isatin−heterodimer complex with the pyrimidoindolone WAY-207890 to assess the affinity and thermodynamics of ligand binding to the unoccupied active site of the complex. Half-site binding is indeed observed (Figure 5D), consistent with WAY-207890 binding at the unoccupied active site. The affinity and thermodynamic profile of WAY-207890 binding to the complex is different from the profile observed upon the binding of WAY-207890 to caspase-3 (Table 3). The affinity for WAY-207890 is reduced, and the enthalpic contribution to binding has increased, consistent with isatin-induced conformational changes in the unoccupied active site upon binding to caspase-3.

Negative Cooperativity of Isatin Binding to Caspase-3 using UV Spectroscopy. The crystal structure of caspase-3 complexed with IST-3 was previously reported, and both active sites are occupied by the ligand (*25*). Results from the above ITC experiments indicated that the isatin affinity of the second active site was greater than 15 μM. UV spectroscopy was next used to monitor the affinity and reactivity of IST1 with caspase-3 by taking advantage of the disappearance of isatin absorbance at 410 nm upon the formation of thiohemiketal at C-3 with the active site cysteine (Figure 6). In the presence of 60 μM caspase-3 heterodimer, no 410 nm absorbance is observed at isatin concentrations below 30 μM. An increase in 410 absorbance is observed at higher isatin concentrations (Figure 6B). The curvature observed at isatin concentrations between 30 and 90 μM is consistent with the decreased potency of the second isatin binding site. The stoichiometry of the interaction can be estimated by two methods: (1) from the intercept of the horizontal axis (56 μM) and (2) the concentration of thiohemiketal formed (68 μM), calculated from the offset of the unreacted IST-1 in the caspase-3 titration from the IST-1 control titration. Both methods for determining the amount of thiohemiketal formed are consistent with two classes of binding sites coupled with thiohemiketal formation resulting in a 1-to-1 stoichiometry. Unfortunately, the difference curve obtained upon subtraction of the caspase titration from the control titration was too noisy to determine the affinity for the second site.

Table 3: Thermodynamic Parameters for Inhibitor Binding to Caspase-3 Determined by Isothermal Titration Calorimetry[a]

inhibitor	buffer	stoichiometry	K_d (nM)	ΔH (kcal/mol)	ΔG (kcal/mol)	$-T\Delta S$ (kcal/mol)
PEP-1[b]	[d]	1.14	81 ± 15	−2.46 ± 0.03	−9.67	−7.21
Ac-DEVD-CHO[b]	[e]	0.97	68 ± 37	−5.66 ± 0.22	−9.77	−4.1
IST-1[b]	[d]	0.63	28 ± 3	−12.04 ± 0.06	−10.3	1.75
IST-2[b]	[d]	0.55	33 ± 3	−10.85 ± 0.08	−10.2	0.64
IST-2[b]	[f]	0.55	28 ± 1	−10.74 ± 0.08	−10.3	0.44
IST-2[b]	[g]	0.60	39 ± 8	−10.83 ± 0.19	−10.1	0.74
WAY-207890[b]	[h]	0.90	8 ± 4	−2.75 ± 0.04	−11.0	−8.20
WAY208698[b]	[h]	0.91	4 ± 2	−0.72 ± 0.02	−10.1	−9.35
WAY-207890[c]	[h]	0.40	275 ± 82	−4.67 ± 0.26	−8.95	−4.28

[a] 25 °C. [b] Titration cell: caspase-3. [c] Titration cell: caspase-IST-1 complex. [d] Assay buffer, 1 mM Cys. [e] Assay buffer, 2 mM DTT. [f] Assay buffer minus sucrose, 5 mM Cys. [g] PBS, 5 mM Cys. [h] Assay buffer, 5 mM Cys.

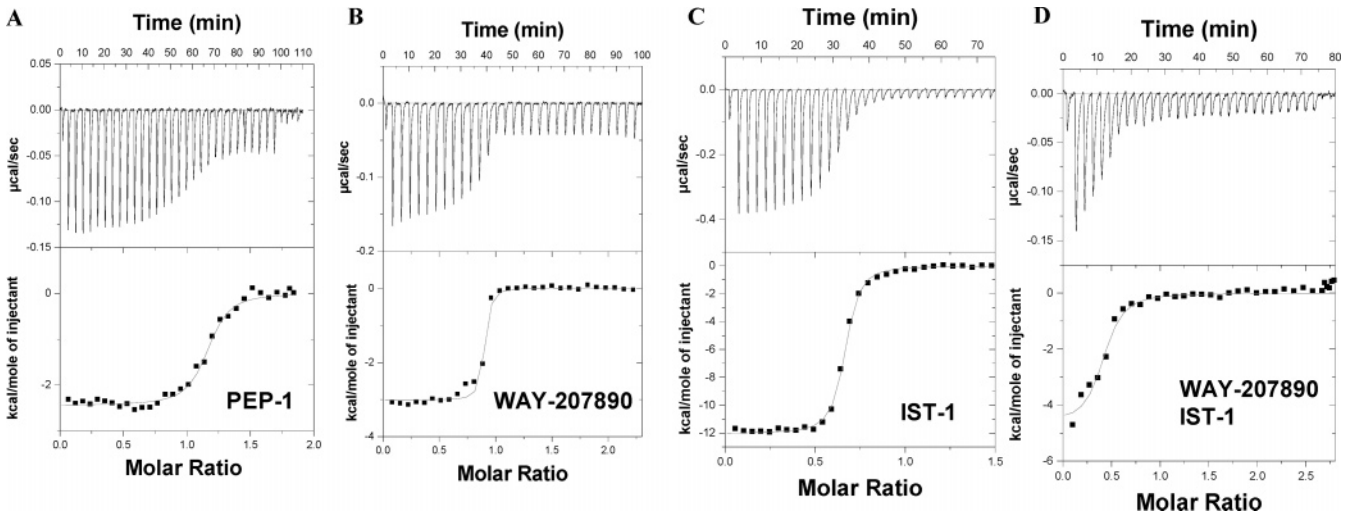

FIGURE 5: Typical ITC curves of caspase-3 and PEP-1 (A), WAY-207890 (B), or IST-1 (C), and the WAY-208698 titration of the IST-1-caspase complex (D). The cell contained 15 μM caspase-3 heterodimer in the assay buffer with 1 mM cysteine and 0.5% DMSO. The syringe contained 150 μM inhibitor solution in the same buffer. Thirty-four injections of 8 μL volume were made at 200 s intervals. Top panels: the raw power traces after baseline correction. Bottom panels: data (■) after peak integration, blank titration substraction, and concentration normalization. The solid line is the least-squares fit of the data to a single binding site model.

DISCUSSION

The central role of caspases in diseases mediated by apoptosis has resulted in much effort to develop small molecule inhibitors of these proteases for therapeutic intervention. Though the mechanism of inhibition and numerous caspase−inhibitor structures have been reported, there have been few reports characterizing the thermodynamics and stoichiometry of inhibitor binding in solution. In the majority of inhibitor−caspase-3 structures reported to date, both active sites of the homodimer have been occupied with covalent bond formation between the active site cysteine and inhibitor carbonyl to yield a symmetric structure. The aim of this study was to obtain additional information about (1) the stoichiometry of both inhibition and binding and (2) the physical nature and thermodynamics of inhibitor interactions to assist inhibitor design.

The stoichiometry of inhibitor interaction with caspase-3 was characterized in this study by a number of different biophysical and biochemical techniques including ITC and active-site titration to correlate ligand binding with functional inhibition. On the basis of reported crystallographic results with peptide−aldehyde and isatin complexes, 1:1 stoichiometry of binding to the active site was expected. Initial results from ITC experiments indicated that the stoichiometry for peptide inhibitor binding was 1:1 as expected. However, isatin binding to caspase-3 was consistent with half-site occupancy. To determine whether the stoichiometry of functional inhibition correlated with the binding stoichiometry, active-site titrations were performed. Caspase-3 was preincubated with the compound and the residual enzyme activity monitored. These experiments confirmed that the stoichiometry of inhibition of caspase-3 by all inhibitors was the same as the stoichiometry of ligand binding. The observation that the active sites of the caspase-3−isatin structure were fully occupied in the crystal structure implied that isatin bound to caspase-3 homodimer with negative cooperativity. Titration calorimetry placed a lower limit on the affinity on the basis of the protein concentration used in the titration (K_{d2} > 15 μM). A UV titration experiment was performed to obtain additional information about the affinity of the second site for isatin by taking advantage of the disappearance of the isatin 410 nm absorbance upon thiohemiketal bond formation. The stoichiometry of the caspase-3−IST-1 complex at high isatin concentration is consistent with the X-ray crystallographic result. On the basis of the lower limit of affinity for the second site from the ITC experiments, isatin binding at the first active site results in a greater than 500-fold loss of potency at the second active site of the homodimer. The reduced potency of the inhibitors in the ITC and fluorescence binding experiments relative to

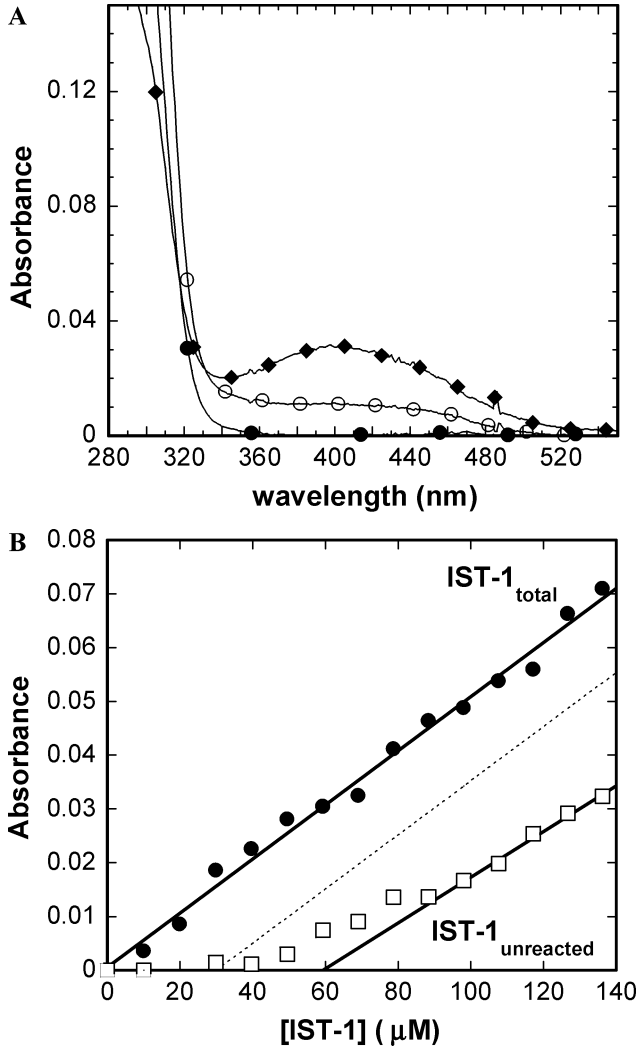

FIGURE 6: UV spectroscopic titration of caspase-3 with IST-1 obtained at 410 nm in assay buffer containing 1 mM cysteine at 22 °C. (A) UV spectra of 60 μM caspase-3 preincubated with 39 μM IST-1 (●) or 78 μM IST-1 (○). The control spectrum of 50 μM IST-1 in buffer is also presented (♦). (B) Titration of 60 μM caspase-3 heterodimer with IST-1. Aliquots of IST-1 were added stepwise to caspase-3 (□) or buffer (●) solution at room temperature, and the absorbance at 410 nm was recorded after the signal maintained a constant value, typically 5 min. The dashed line corresponds to the expected signal for half-site reactivity.

the steady-state K_i derived from inhibition kinetics may be attributed to the binding experiments monitoring an initial binding event.

Consistent with a conformational change induced upon isatin binding are the results from the fluorescence binding experiments. Caspase-3 contains two Trp residues in the active site that are base-stacked in crystal structures of caspase-3 complexes. Though base-stacking of the Trp residues was observed in the unoccupied active site of a partially occupied complex of caspase-9 with peptide inhibitor (*26*), conformational changes are observed in the active site and surrounding loop regions of apo and bound caspase-3 (*12*). Significant Trp quenching is observed upon inhibitor binding, consistent with a change in water structure and/or a conformational change. The extent of quenching observed in this study is in contrast to the results reported for the interaction of the irreversible inhibitor Z-VAD-FMK with procaspase-3 (*27*), where little Trp fluorescence quenching was observed upon inhibitor binding. In our study, a similar extent of Trp fluorescence quenching was observed for all classes of inhibitors, which indicated that the quenching was likely not due to compound interference or the polarity of the inhibitor (Ac-DEVD-CHO vs PEP-1) but reflected ligand-induced conformational changes in the Trp environment. We speculate that ligand-induced rearrangement of loops L1−L4 surrounding the active site perturb Trp fluorescence through local changes in water structure and changes in proximity of the Trp side chains to the active site C170, a potential quencher (*28*). Attempts were made to characterize the conformational change by circular dichroism but were not successful because of the presence of the reducing agent.

To further characterize the changes induced in the second active site of the caspase-3 homodimer upon isatin binding, we performed a titration calorimetry experiment with the isatin−caspase-3 complex to obtain a thermodynamic characterization of the second active site. The pyrimidoindolone WAY-207890 inhibitor was titrated into the isatin−caspase-3 complex, and stoichiometric binding to the second active site was observed. Competition of the pyrimidoindolone for bound isatin was ruled out, as the predicted net heat released upon binding would be endothermic (*29*). The WAY-207890 affinity for the unoccupied active site was decreased approximately 34-fold relative to the affinity obtained from the caspase-3-WAY-207890 titration. WAY-207890 binding to the isatin complex was also more enthalpic, consistent with isatin-induced conformational changes in the unoccupied active site. This result was rather unexpected because the active sites in the homodimer are significantly far apart and opposed in the homodimer structure. However, large conformational changes are observed in the crystal structure of the caspase-7 allosteric inhibitor that binds at the homodimer interface and distorts both active sites, resulting in the loss of substrate binding and catalysis (*15*). Thus, conformational changes induced in a caspase active site and/or loop(s) are readily transmitted to other domains of the protein.

Though the affinities of the isatin and pyrmidoindolone inhibitors listed in Tables 2 and 3 are similar, the magnitude and proportion of enthalpy contributions to binding affinity are significantly different (Table 3). Especially interesting is the significant thermodynamic profile difference between the structurally similar isatin and pyrimidoindolone analogues, implying a different mode of binding. However, no significant differences were observed upon comparison of the crystal structures of the isatin and PI complexes in which the inhibitor occupies both active sites (data not shown). The reproducibility of the isatin thermodynamic profile in different buffers eliminated the possibility of the contribution of proton-transfer reactions to the isatin binding enthalpy. No change in association state upon ligand binding was observed in sedimentation velocity experiments (data not shown), which ruled out energetic contributions from caspase-3 association or dissociation. As noted previously by Lee et al. (*19*) and in our experiments, isatins rapidly reacted with caspase-3 to form the thiohemiketal. Upon addition of isatin to caspase-3, isatin absorbance at 410 nm disappeared within 1 min, consistent with rapid thiohemiketal formation. Thus, the heat of thiohemiketal formation would contribute to the observed enthalpy during the time of isatin injection and the delay period between injections in the ITC experiments. A

comparison of the energetics of the bonds broken (C−O, +85.5 kcal/mol; S−H, 81 kcal/mol) with the bonds formed (C−S, 65.0 kcal/mol; O−H, 111.0, kcal/mol) indicates that the net process of thiohemiketal formation would be exothermic with approximately 11 kcal/mol liberated upon covalent bond formation. Though the pyrimdoindolones react more slowly with cysteine to form the thiohemiketal (as measured by changes in the UV spectrum at 450 nm), a similar heat of reaction would be expected to contribute to the enthalpy of pyrimidoindolone binding to caspase-3. However, the slow heat release from chemical reaction may be masked as a baseline drift during the course of the PI titration. Significantly less heat is observed with WAY-207890 binding relative to the isatins, and favorable entropic contributions are observed. The favorable entropy observed upon the binding of pyrimidoindolones or peptidomimetics is consistent with increased van der Waals interactions that would arise from the release of water molecules from the binding interface. The contributions to the enthalpy of isatin binding to caspase-3 are more complex. Fluorescence quenching experiments, the titration calorimetry experiment of the isatin−caspase-3 complex with pyrimidoindolone, and the negative cooperativity of isatin binding clearly indicate that conformational changes in the unoccupied binding site have occurred. The negative entropy observed upon isatin binding is consistent with conformational reorganization and loss of configurational entropy in caspase-3 (*30*). Thus, the observed heat released in isatin titration would be the sum of the contributions from binding, conformational change, and thiohemiketal formation.

In summary, though numerous caspase−inhibitor structures and mechanism of inhibition studies have been performed, not much information has been reported about the stoichiometry of inhibition and thermodynamics of inhibitor binding that would aid inhibitor design. A structure-based approach to target the active site cysteine with compounds containing a reactive electrophilic center is the main strategy used to design potent caspase inhibitors (*8*−*10*). Though only caspase-3 complexes with both active sites occupied by inhibitor have been reported, our studies demonstrate that occupancy at one site can result in a conformational change and inhibition of the enzyme activity concomitant with reduced affinity for the second active site. Information about the conformation of the asymmetric complex is likely lost in structural studies because of the high concentration of protein and the excess quantity of inhibitor present resulting in the formation of the symmetric complex. Exactly what causes the conformational change to form the asymmetric isatin−caspase-3 complex is an open question, and additional studies are required to answer it. Our study further indicates that though two chemical series may appear structurally similar both in solution and complexed to protein, significant differences exist in the mode of binding of the different ligands that are not readily apparent in the crystal structures but can be readily distinguished by biochemical and biophysical methods.

SUPPORTING INFORMATION AVAILABLE

Figures showing the inhibition kinetics of caspase-3 in the presence of different inhibitors (Figure 1), active-site titration for PEP-1, WAY-208698, and IST-2 (Figure 2), and the binding isotherm for Ac-DEVD-CHO derived from changes in intrinsic Trp fluorescence (Figure 3). This material is available free of charge via the Internet at http://pubs.acs.org.

REFERENCES

1. Jacobson, M. D., Weil, M., and Raff, M. C. (1997) Programmed cell death in animal development, *Cell 88*, 347−354.
2. Thornberry, N. A., and Lazebnik, Y. (1998) Caspases: enemies within, *Science 281*, 1312−1316.
3. Denault, J. B., and Salvesen, G. S. (2002) Caspases: keys in the ignition of cell death, *Chem. Rev. 102*, 4489−4499.
4. Siegel, R. M. (2006) Caspases at the crossroads of immune-cell life and death, *Nat. Rev. Immunol. 6*, 308−317.
5. Baliga, B. C., Read, S. H., and Kumar, S. (2004) The biochemical mechanism of caspase-2 activation, *Cell Death Differ. 11*, 1234−1241.
6. Pop, C., Timmer, J., Sperandio, S., and Salvesen, G. S. (2002) The apoptosome activates caspase-9 by dimerization, *Mol. Cell 22*, 269−275.
7. Yin, G., Park, H. H., Chung, J. Y., Lin, S. C., Lo, Y. C., da Gracia, L. S., Jiang, X., and Wu, H. (2006) Caspase-9 holoenzyme is a specific and optimal procaspase-3 processing machine, *Mol. Cell 22*, 259−268.
8. Ashwell, S. (2001) Recent advances in small molecule inhibitors, *Exp. Opin. Ther. Patents 11*, 1593.
9. O'Brien, T., and Lee, D. (2004) Prospects for caspase inhibitors, *Mini-Rev. Med. Chem. 4*, 153−165.
10. Linton, S. D. (2005) Caspase Inhibitors: A pharmaceutical industry perspective, *Curr. Top. Med. Chem. 5*, 1697−1717.
11. Romanowski, M. J., Scheer, J. M., O'Brien, T., and McDowell, R. S. (2004) Crystal structures of a ligand-free and malonate-bound Human Caspase-1. Implications for the mechanism of substrate binding, *Structure 12*, 1361−1371.
12. Ni, C. Z., Li, C., Wu, J. C., Spada, A. P., and Ely, K. R. (2003) Conformational restrictions in the active site of unliganded human caspase-3, *J. Mol. Recognit. 16*, 121−124.
13. Chai, J., Wu, Q., Shiozaki, E., Srinivasula, S. M., Alnemri, E. S., and Shi, Y. (2001) Crystal structure of a procaspase-7 zymogen: mechanisms of activation and substrate binding, *Cell 107*, 399−407.
14. Fuentes-Prior, P., and Salvesen, G. S. (2004) The protein structures that shape caspase activity, specificity, activation and inhibition, *Biochem. J. 384*, 201−232.
15. Hardy, J. A., Lam, J., Nguyen, J. T., O'Brien, T., and Wells, J. A. (2004) Discovery of an allosteric site in the caspases, *Proc. Natl. Acad. Sci. U.S.A. 101*, 12461−12466.
16. Scheer, J., Romanowski, M. J., and Wells, J. A. (2006) A common allosteric site and mechanism in caspases, *Proc. Natl. Acad. Sci. U.S.A. 103*, 7595−7600.
17. Laue, T. M., Shah, B. D., Ridgeway, T. M., and Pelletier, S. L. (1992) in *Analytical Ultracentrifugation in Biochemistry and Polymer Science* (Harding, S. E., Rowe, A. J., and Horton, J. C., Eds.) pp 90−125, Royal Society of Chemistry, Cambridge, U.K.
18. Garcia-Calvo, M., Peterson, E. P., Leiting, B., Ruel, R., Nicholson, D. W., and Thornberry, N. A. (1998) Inhibition of human caspases by peptide-based and macromolecular inhibitors, *J. Biol. Chem. 273*, 32608−32613.
19. Lee, D., Long, S. A., Murray, J. H., Adams, J. L., Nuttall, M. E., Nadeau, D. P., Kikly, K., Winkler, J. D., Sung, C. M., Ryan, M. D., Levy, M. A., Keller, P. M., and DeWolf, W. E. (2001) Potent and selective nonpeptide inhibitors of caspases 3 and 7, *J. Med. Chem. 44*, 2015−2026.
20. Morrison, J. F., and Walsh, C. T. (1988) The behavior and significance of slow-binding enzyme inhibitors, *Adv. Enzymol. Relat. Areas Mol. Biol. 61*, 201−301.
21. Fukada, H., and Takahashi, K. (1998) Enthalpy and heat capacity changes for the proton dissociation of various buffer components in 0.1 M potassium chloride, *Proteins 33*, 159−166.
22. Semple, G., Ashworth, D. M., Baker, G. R., Batt, A. R., Baxter, A. J., Benzies, D. W. M., Elliot, L. H., Evans, M., Franklin, R. J., Hudson, P., Jenkins, P. D., Pitt, G. R., Rooker, D. P., Sheppard, A., Szelke, M., Yamamoto, S., and Isomura, Y. (1997) Pyridone-based peptidomimetic inhibitors of interleukin-1-β-converting enzyme (ICE), *Bioorg. Med. Chem. Lett. 7*, 1337−1342.
23. Dollings, P. J., Aulabaugh, A., Banker, A., Chan, H., Cho, S., Cowling, R., Dietrich, A., Di, L., Ellestad, G., Fennell, M., Huang, X., Hum, W. T., Huryn, D., Jin, G., Kapoor, B., Kleintop, T., LaRocque, J., Ling, H. P., Marathias, V., Moy, F., Petusky, S.,

Somers, W. S., Tawa, G. J., Tsao, D., Wood, A., and Xu, W. (2005) Identification and characterization of 3,4-dihydro-2H-pyrimido(1,2-a)indol-10-ones as caspase inhibitors, *Abstracts of Papers*, 230th National Meeting of the American Chemical Society, Washington, DC, AN 2005:739825.

24. Cha, S. (1975) Tight-binding inhibitors. I. Kinetic behavior, *Biochem. Pharmacol. 24*, 2177−2185.
25. Lee, D., Long, S. A., Adams, J. L., Chan, G., Vaidya, K. S., Francis, T. A., Kikly, K., Winkler, J. D., Sung, C. M., Debouck, C., Richardson, S., Levy, M. A., DeWolf, W. E., Keller, P. M., Tomaszek, T., Head, M. S., Ryan, M. D., Haltiwanger, R. C., Liang, P. H., Janson, C. A., McDevitt, P. J., Johanson, K., Concha, N. O., Chan, W., Abdel-Meguid, S. S., Badger, A. M., Lark, M. W., Nadeau, D. P., Suva, L. J., Gowen, M., and Nuttall, M. E. (2000) Potent and selective nonpeptide inhibitors of caspases-3 and -7 inhibit apoptosis and maintain cell functionality, *J. Biol. Chem. 275*, 16007−16014.
26. Renatus, M., Stennicke, H. R., Scott, F. L., Liddington, R. C., and Salvesen, G. S. (2001) Dimer formation drives the activation of the cell death protease caspase 9, *Proc. Natl. Acad. Sci. U.S.A. 98*, 14250−14255.
27. Bose, K., Pop, C., Feeney, B., and Clark, A. C. (2003) An uncleavable procaspase-3 mutant has a lower catalytic efficiency but an active site similar to that of mature caspase-3, *Biochemistry 42*, 12298−12310.
28. Chen, Y., and Barkley, M. D. (1998) Toward understanding tryptophan fluorescence in proteins, *Biochemistry 37*, 9976−9982.
29. Sigurskjold, B. W. (2000) Exact analysis of competition ligand binding by displacement isothermal titration calorimetry, *Anal. Biochem. 277*, 260−266.
30. Ward, W. H. J., and Holdgate, G. A. (2001) Isothermal titration calorimetry in drug discovery, *Prog. Med. Chem. 38*, 309−376.

BI7000505